doi:10.3788/gzxb20134208.0891

哈达玛光谱仪能量偏移的修正算法

王峥杰[1,2],杜云飞[1],胡炳樑[1],刘磊[1],孔亮[1],闫鹏[1],武琪敬[1]
(1 中国科学院西安光学精密机械研究所,西安 710119)
(2 中国科学院大学,北京 100049)

摘 要:介绍了采用数字微镜器件的哈达玛光谱仪的成像原理及光学结构,阐述了数字微镜器件像元大小与探测器阵列尺寸不匹配,从而导致光谱能量偏移的现象.通过对复原图像进行修正,提出了矩阵修正算法.采用由哈达玛光谱仪得到的 7 阶植物光谱图像,对复原图像应用矩阵修正算法进行修正,有效减小了明暗条纹现象.为了提高复原图像的成像质量,实验选取相邻明暗条纹中的点绘制光谱曲线图,结果表明:存在能量偏移的暗条纹处的光谱曲线偏移较大,明条纹处光谱曲线基本重合,证明了修正算法的有效性.

关键词:能量偏移;修正矩阵;哈达玛变换;数字微镜器件
中图分类号:TP751.1 **文献标识码**:A **文章编号**:1004-4213(2013)08-0891-6

A Correction Algorithm on Reducing Energy Excursion Phenomenon

WANG Zheng-jie[1,2], DU Yun-fei[1], HU Bing-liang[1], LIU Lei[1],
KONG Liang[1], YAN Peng[1], WU Qi-jing[1]
(1 *Xi'an Institute of Optics and Precision Mechanics of Chinese Academy of Sciences, Xi'an* 710119, *China*)
(2 *Graduate University of Chinese Academy Sciences, Beijing* 100049, *China*)

Abstract: The imaging principle and the structure of a Hadamard transform spectral imager with a digital micro-mirror device are presented. A phenomenon of energy excursion which is caused by mismatching of the mask unit size and the detector pixel size is expatiated. To fix the recovery images, a matrix correction algorithm is proposed. The 7-order images of plants acquired by the Hadamard transform spectral imager are used and the correction algorithm is operated on the recovery images with error, which reduces the phenomenon of dark stripes effectively. In order to improve the image quality of the recovery images, two dots in and off two adjacent dark stripes are selected to show the spectrum curves. The results show the close spectrum curves of the dot off dark stripes and the different curves of the dot in dark stripes. The comparison illustrates the validity of the correction algorithm.

Key words: Energy excursion; Correction matrix; Hadamard transform; Digital Micro-mirror Device (DMD)

0 Introduction

Hadamard Transform (HT) spectral technology[1] is a novel spectral modulation technique developed in recent decades. It can obtain spatial and spectral information of the target, and has been widely used in fields of spectral data acquisition, target recognition and classification, weak signal detection, etc.[2] Imaging spectrometer based on HT theory which has advantages of high energy input, single detector multi-channel imaging ability through

Foundation item: The National Natural Science Foundation of China (No. 40805013)
First author: WANG Zheng-jie (1987—), male, postgraduate student, M.S. degree, mainly focuses on spectral images processing. Email: zjwang1987@gmail.com
Responsible author(Corresponding author): HU Bing-liang (1976—), male, professor, Ph.D. degree, mainly focuses on spectral imaging technology and high-speed signal processing. Email: hbl@opt.ac.cn
Received: Feb. 22, 2013; **Accepted**: May. 16, 2013

single detector and high signal-to-noise ratio.[3]

Programmable mask, which is used to accomplish space and spectrum coding, is the key component of the Hadamard Transform Spectral Image(HTSI).[4] The HTSI introduced here uses Digital Micro-mirror Device (DMD) as the programmable mask. Due to the different sizes of the mask unit and detector pixel, energy excursion phenomenon occurs to reduce the quality of recovery images.

There are a mass of ways to process spectral images. The representative methods are, space-frequency filtering, histogram matching[5], principal components analysis, moment matching[6], etc. In our laboratory, spectral revision algorithm[3] and modified linear interpolation algorithm[7] are used in previous work to improve the spectral images. In this experiment, to improve the energy excursion phenomenon, a new correction matrix for the recovery images is proposed and used to ameliorate the recovery images.

1 Principle and structure of HTSI

An engineering prototype[8] of Hadamard transform spectral imager for object detection is built at the Key Laboratory of Spectral Imaging Technology of Chinese Academy of Sciences. The prototype works in the visible band ranged from 550 nm to 680 nm and is composed with five parts named foreoptics, dispersing system, spatial light modulator (DMD), assembling system and acquisition module. The dispersing system and assembling system are consist of refractive lens and the spatial light modulator(DMD) treated as the blazed diffraction grating and the programmable mask, is set on the second image plane to implement the function of spectral domain encoding. Fig. 1 shows the optical system of the HT spectral imager.

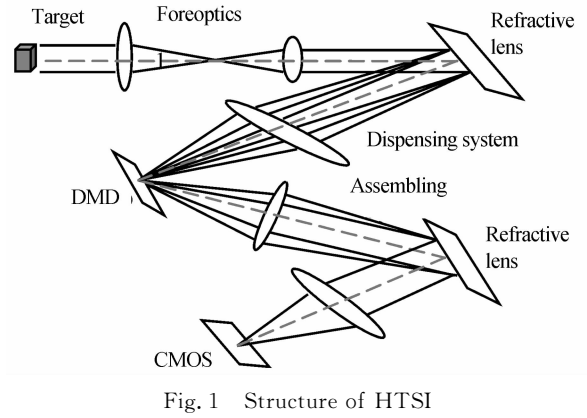

Fig. 1 Structure of HTSI

Light from the detected object is imaged on to a focal plane, dispersed, and reimaged onto a DMD that selects specific spectral and spatial regions of the dispersed image. The reflected light is then recombined to form a polychromatic image on a detector.[9] Images are obtained through time modulation for setting the mask encoding information.

2 Coding theory of HT

HT mask is the key to HT imaging principle. For a mask of n units, the detected signal y is

$$y_j=\sum_{i=1}^{n}S_{ij}X_i \tag{1}$$

where y_j is light energy modulated by mask j, and X_i is the energy of the element i on the mask. It can be written in matrix form.

$$\boldsymbol{Y}=\boldsymbol{S}\cdot\boldsymbol{X} \tag{2}$$

In the experiments, HTSI based on DMD uses the 7-order mask. Namely, the matrix $\boldsymbol{S}$ is a 7-order square matrix.

$$\boldsymbol{S}=\begin{bmatrix}1&1&1&0&1&0&0\\1&1&0&1&0&0&1\\1&0&1&0&0&1&1\\0&1&0&0&1&1&1\\1&0&0&1&1&1&0\\0&0&1&1&1&0&1\\0&1&1&1&0&1&0\end{bmatrix} \tag{3}$$

The spectrum information of the recovery image is obtained by using $\boldsymbol{S}^{-1}$, the inverse matrix of $\boldsymbol{S}$.

$$\boldsymbol{X}=\boldsymbol{S}^{-1}\cdot\boldsymbol{Y} \tag{4}$$

3 Emergence of energy excursion

The encoding mask used in the experiment is a 7th-order square matrix, and composed by the one-dimensional left cyclic code [1 1 1 0 1 0 0]. The mask is shown in Fig. 2.

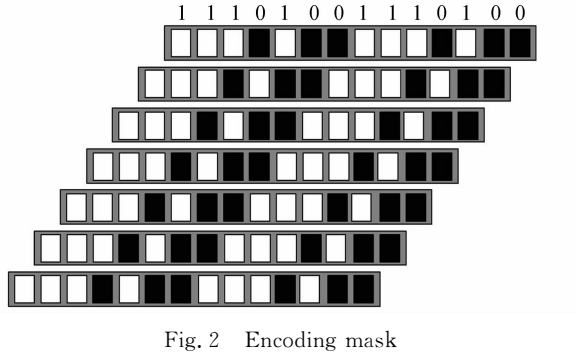

Fig. 2 Encoding mask

Theoretically, light imaged on to the detector is modulated and encoded by the mask strictly. According to the mask, pixel j is encoded as

$$y_1=x_1+x_2+x_3+0\times x_4+x_5+0\times x_6+0\times x_7 \quad (5)$$

Based on the composing of HT spectral imager in part II, the spatial light modulator in our system is DMD[10] (a patented product Discovery™ 0.55XGA) produced by Texas Instruments which is a key to the encoding module. It can be programmed to generate a dynamic series of spatial patterns that implement the transform functions[11]. The detector is a CMOS imager sensor[12] that integrates the functionality of complete analog image acquisition, digitizer and digital signal processing system on a single chip named IBIS5-B-1300 produced by Cypress Semiconductor Corporation.

The DMD has an 1 024 × 768 array of aluminum in 10.8 μm micro-mirror pitch. And detector selected in our system contains 1 280 × 1 024 square pixels of 6.7 × 6.7 mm^2 each. Obviously, they do not match each other. The encoded lights pass through the assembling system and image on the CMOS detector which can't cover the corresponding pixels. Some parts of the assembling light's energy is mapping on two adjacent pixels which causes energy reducing periodically. It is the phenomenon of energy excursion[13-14] which is shown in Fig. 3 and it reduces the quality of spectral images and the veracity of object detection.

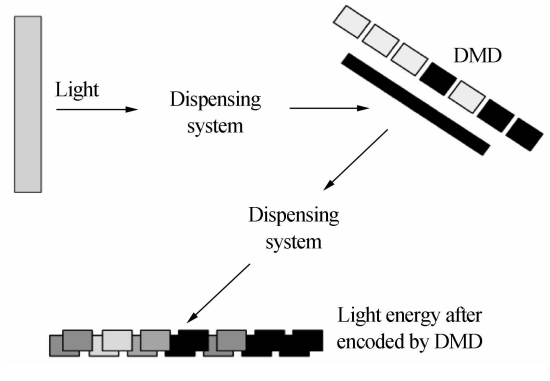

Fig. 3　Energy excursion

Assuming the light energy through pixels in every mask is uniform, the excursion of every pixel is same. Pixel $j+1$ is encoded as

$$\begin{aligned} y_1=&(1-\delta)x_1+(\delta\cdot x_1+(1-\delta)x_2)+(\delta\cdot x_2+(1-\delta)x_3)+(0\cdot x_3+0\cdot x_4)+(\delta\cdot x_4+(1-\delta)x_5)+(0\cdot x_5+0\cdot x_6)+(0\cdot x_6+0\cdot x_7)+\delta\cdot x_7=\\ &x_1+x_2+(1-\delta)x_3+\delta\cdot x_4+(1-\delta)x_5+0\cdot x_6+\delta\cdot x_7 \end{aligned} \quad (6)$$

where δ is energy excursion. A new coding form, based on mask $\boldsymbol{H}$, can be expressed in (6).

$$\begin{bmatrix} y_1\\ y_2\\ y_3\\ y_4\\ y_5\\ y_6\\ y_7 \end{bmatrix}=\begin{bmatrix} 1 & 1 & 1-\delta & \delta & 1-\delta & 0 & \delta\\ 1 & 1-\delta & \delta & 1-\delta & 0 & \delta & 1\\ 1-\delta & \delta & 1-\delta & 0 & \delta & 1 & 1\\ \delta & 1-\delta & 0 & \delta & 1 & 1 & 1-\delta\\ 1-\delta & 0 & \delta & 1 & 1 & 1-\delta & \delta\\ 0 & \delta & 1 & 1 & 1-\delta & \delta & 1-\delta\\ \delta & 1 & 1 & 1-\delta & \delta & 1-\delta & 0 \end{bmatrix}\cdot \begin{bmatrix} x_1\\ x_2\\ x_3\\ x_4\\ x_5\\ x_6\\ x_7 \end{bmatrix} \quad (7)$$

That is $\boldsymbol{Y}=\boldsymbol{HX}$. Inversing transform of Eq. (7), the recovery image is $\boldsymbol{X}=\boldsymbol{H}^{-1}\boldsymbol{Y}$.

Due to the difference of encoding matrix and recovery matrix, dark stripes emerge in the standard recovery images recovered by Eq. (4) which exists energy excursion phenomenon. This is the main reason discussed in this paper, without considering other possible reasons like device response difference and slit width uneven, etc.[15] To improve the quality of the spectral image, a correction matrix is proposed to amend the standard recovery images and reduce this phenomenon.

4　Correction algorithm derivation

Theoretical coding matrix $\boldsymbol{S}$ is given in Eq. (3). Because of the limitation of the hardware equipment, errors may emerge by energy excursion. Therefore the actual coding matrix is given in Eq. (7). Split the matrix $\boldsymbol{H}$

$$\boldsymbol{Y}=\begin{bmatrix} y_1\\ y_2\\ y_3\\ y_4\\ y_5\\ y_6\\ y_7 \end{bmatrix}=\begin{bmatrix} 1 & 1 & 1 & 0 & 1 & 0 & 0\\ 1 & 1 & 0 & 1 & 0 & 0 & 1\\ 1 & 0 & 1 & 0 & 0 & 1 & 1\\ 0 & 1 & 0 & 0 & 1 & 1 & 1\\ 1 & 0 & 0 & 1 & 1 & 1 & 0\\ 0 & 0 & 1 & 1 & 1 & 0 & 1\\ 0 & 1 & 1 & 1 & 0 & 1 & 0 \end{bmatrix}\begin{bmatrix} x_1\\ x_2\\ x_3\\ x_4\\ x_5\\ x_6\\ x_7 \end{bmatrix}+$$

$$\delta\begin{bmatrix} 0 & 0 & -1 & 1 & -1 & 0 & 1\\ 0 & -1 & 1 & -1 & 0 & 1 & 0\\ -1 & 1 & -1 & 0 & 1 & 0 & 0\\ 1 & -1 & 0 & 1 & 0 & 0 & -1\\ -1 & 0 & 1 & 0 & 0 & -1 & 1\\ 0 & 1 & 0 & 0 & -1 & 1 & -1\\ 1 & 0 & 0 & -1 & 1 & -1 & 0 \end{bmatrix}\begin{bmatrix} x_1\\ x_2\\ x_3\\ x_4\\ x_5\\ x_6\\ x_7 \end{bmatrix}=$$

$$\boldsymbol{HX}=\boldsymbol{SX}+\delta\boldsymbol{QX} \quad (8)$$

where matrix $\boldsymbol{Q}$ is the coefficient matrix for the excursion δ, and it′s a non-invertible matrix. Multiply Eq. (8) both sides with $\boldsymbol{S}^{-1}$

$$\boldsymbol{S}^{-1}\boldsymbol{Y}=\boldsymbol{X}+\delta\boldsymbol{S}^{-1}\boldsymbol{Q}\boldsymbol{X} \tag{9}$$

The recovery images with energy excursion are acquired by the standard mask

$$\boldsymbol{X}'=\boldsymbol{S}^{-1}\boldsymbol{Y} \tag{10}$$

Use Eq. (10) to substitute $\boldsymbol{S}^{-1}\boldsymbol{Y}$

$$\boldsymbol{X}'=\boldsymbol{X}+\delta\boldsymbol{S}^{-1}\boldsymbol{Q}\boldsymbol{X} \tag{11}$$

and obtain the recovery images after correction

$$\boldsymbol{X}=\boldsymbol{R}\cdot\boldsymbol{X}' \tag{12}$$

where $\boldsymbol{X}'$ is the recovery image with energy excursion, the correction matrix $\boldsymbol{R}$ is

$$\boldsymbol{R}=\begin{bmatrix}1-\delta & 0 & 0 & 0 & 0 & 0 & \delta\\ \delta & 1-\delta & 0 & 0 & 0 & 0 & 0\\ 0 & \delta & 1-\delta & 0 & 0 & 0 & 0\\ 0 & 0 & \delta & 1-\delta & 0 & 0 & 0\\ 0 & 0 & 0 & \delta & 1-\delta & 0 & 0\\ 0 & 0 & 0 & 0 & \delta & 1-\delta & 0\\ 0 & 0 & 0 & 0 & 0 & \delta & 1-\delta\end{bmatrix}^{-1} \tag{13}$$

5 Algorithm validity and experiment analysis

5.1 Algorithm validity

A data source $x=[96\ 105\ 108\ 98\ 77\ 80\ 99]^{\mathrm{T}}$ which is similar to the original data is used to validate the correction algorithm. It is assumed that the actual coding matrix is composed by one-dimensional left cyclic code [1 1 0.7 0.3 0.7 0 0.3]. The relative average error (RAE) $\xi=\sqrt{\sum_{j=1}^{j=7}(X_{1or2}^{2}(j)-X^{2}(j))/7}$ is used to show the comparison of the recovery images $\boldsymbol{X}_2$ with energy excursion and the correction recovery images $\boldsymbol{X}_1$.

Table 1 Comparison of RAE

δ	ξ_1 of X_1	ξ_2 of X_2
0	21.719 2	21.719 2
0.1	19.251 2	21.719 2
0.2	14.342 1	21.719 2
0.3	0	21.719 2
0.4	18.230 8	21.719 2
0.5	22.916 5	21.719 2
0.6	27.987 8	21.719 2
0.7	29.464 8	21.719 2
0.8	30.611 5	21.719 2
0.9	31.385 9	21.719 2
1	33.245 9	21.719 2

The table above shows that the recovery images after correction have a smaller RAE and are much closer to the original data. It means the correction matrix is able to repair the recovery images with energy excursion and has better spectral recovery precision.

5.2 Experimental analysis

The 7-order plants images is acquired by HT imager in the experiment. Fig. 4 shows the recovery images of 7 orders from 550 nm to 680 nm that are using the standard recovery matrix. It is obviously to see many dark stripes in the recovery images due to the energy excursion.

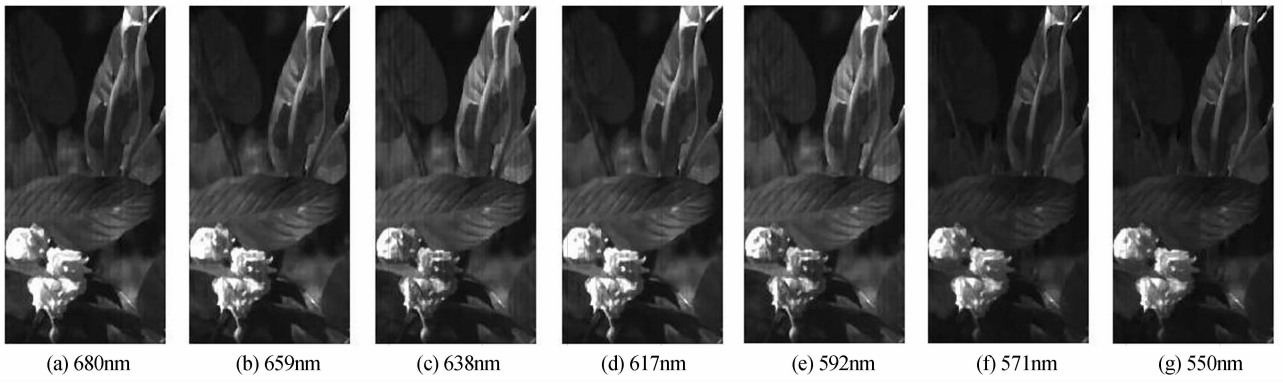

Fig. 4 Recovery images with energy excursion

Use Eq. (12) to amend the recovery images with error above by using the correction matrix $\boldsymbol{R}$, and acquire the recovery images of 7 orders from 550 nm to 680 nm after correction which are shown in Fig. 5. The dark stripes in the recovery images after correction by matrix $\boldsymbol{R}$ can hardly see. To see the comparison clearly, enlarge the part of the flowers for further observation and show in Fig. 6. Evidently, dark stripes in the recovery images after correction are reduced significantly, and even non-existent.

Three of the recovery images of band 659 nm, 592 nm and 571 nm are selected to form a synthesized image. It can be clearly seen in Fig. 7, after modification by correction matrix, the dark stripes caused by energy excursion are markedly improved, and greatly improved the quality of the recovery images.

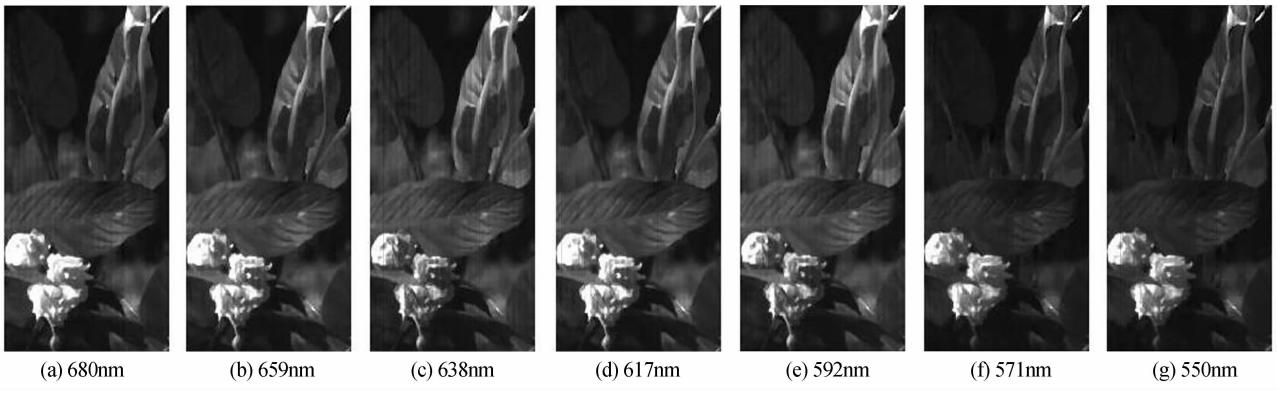

Fig. 5　Recovery images after correction

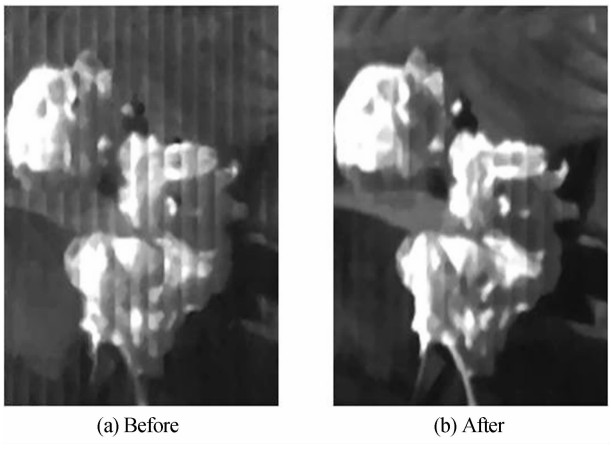

Fig. 6　Comparison of 7-order images

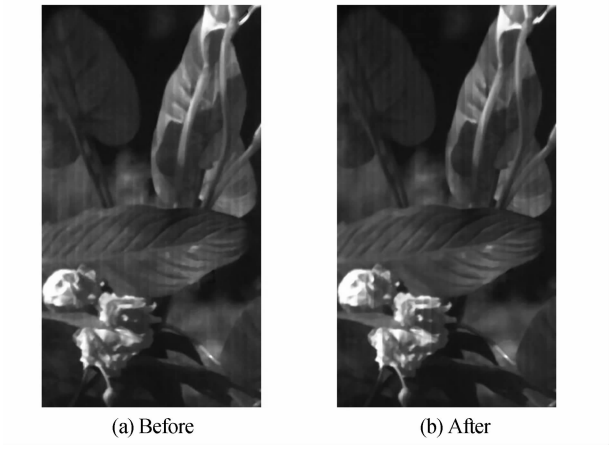

Fig. 7　Comparison of synthesized images

As is known to all, spectrum curves explain the recovery of spectral images intuitively. The spectrum curves of two dots in and off two adjacent dark stripes that are in the yellow box in Fig. 8 are shown in Fig. 9 to see the changes of the spectrum curves before and after correction.

The spectrum curves of the dot off dark stripes shown in Fig. 9(b) are close in recovery images before and after correction. In Fig. 9(a), the spectrum curves are obviously different in dark stripes. The comparison shows the great correction effect on the stripes of the recovery images when using the correction matrix. It enhances the spectral imaging quality significantly.

Fig. 8　Two dots in and off two adjacent dark stripes

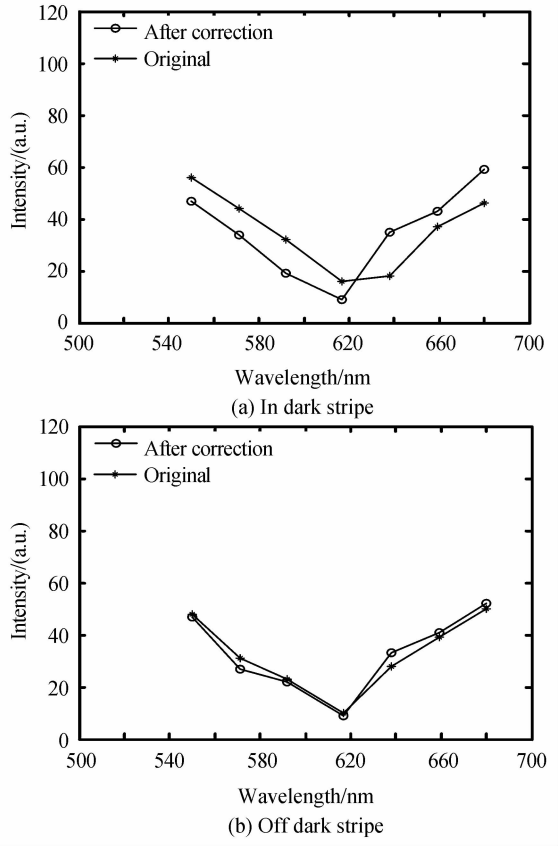

Fig. 9　Spectrum curves in and off dark stripe

6　Conclusion

This paper expatiates the HT theory and discusses the energy excursion phenomenon caused by mismatching of DMD slit size and the detector

pixel size. To improve the imaging quality, a correction algorithm is proposed to correct the recovery images with energy excursion. Moreover, experiments also explain the validity of the correction matrix.

References

[1] HARWIT J V, SLONE N J. Hadmard transform optics[M]. New York: Academic Press, 1979.

[2] YIN Shi-min, JI Zhong-ying, XUI Yan, *et al*. Research on pixel response non-uniformity correction of CCD in interferential imaging spectrometer [J]. *Acta Photonica Sinica*, 2009, **38**(4): 880-884.

[3] ZHOU Jin-song, LV Qun-bo, XIANGLI Bin. Analysis and revision on spectra aliasing of hadamard transform spectral imager[J]. *Acta Photonica Sinica*, 2005, **34**(10): 1518-1521.

[4] JIA Hui, YAO Yong. Analysis of corresponding changes of two dimensional hadamard spectral images caused by imperfect encoding templates and their position errors [J]. *Acta Photonica Sinica*, 2007, **36**(2): 294-299.

[5] WEGENER M J. Destriping multiple sensor imagery by improved histogram matching[J]. *International Journal of Remote Sensing*, 1999, **11**(5): 859-875.

[6] GADALLAH F L, CSILLAG F. Destriping multisensory imagery with moment matching[J]. *International Journal of Remote Sensing*, 2000, **21**(12): 2505-2511.

[7] LI Xiang-juan, YANG Jian-feng, XUE Bin. Destriping IIM images with modified linear interpolation algorithm[J]. *Acta Photonica Sinica*, 2010, **39**(1):164-168.

[8] SUN Xin, HU Bing-liang, LI Li-bo, *et al*. An engineering prototype of hadamard transform spectral imager based on digital micro-mirror device[J]. *Optics & Laser Technology*, 2012, **44**(2012): 210-217.

[9] GOLDSTEIN N, VUJKOVIC-CVIJIN P, FOX M, *et al*. DMD-based adaptive spectral imagers for hyperspectral imagery and direct detection of spectral signatures[C]. *SPIE*, 2009, **7210**: 721008.

[10] TEXAS Instruments. 0.55XGAChipset [EB]. (2010-9), [2012-2]. http://focus.ti.com.cn/cn/paramsearch/docs/parametricsearch.tsp?family=analog&familyId=1746&uiTemplateId=MDLP_PARMSRCH_T&paramCriteria=no.

[11] VUJKOVIC-CVIJIN P, GOLDSTEIN N, FOX M, *et al*. Adaptive spectral imager for space-based sensing[C]. *SPIE*, 2006, **6206**: 62060X.

[12] CYPRESS Semiconductor corporation. 1.3 MP CMOS image sensor[EB]. (2007-1-11)www.onsemi.com/pub/Collateral/NOII5SM1300A-D.PDF.

[13] YAN Peng, HU Bing-liang, LIU Xue-bin, *et al*. Hadamard transform spectrometer mixed pixels' unmixing method[J]. *Spectroscopy and Spectral Analysis*, 2011, **31**(10): 2870-2873.

[14] XU Jun, HU Bing-liang, FENG Da-zheng, *et al*. Analysis and study of the interlaced encoding pixels in Hadamard transform spectral imager based on DMD[J]. *Optics and Lasers in Engineering*, 2012, **50**(2012): 458 - 464.

[15] CAO Wei-liang, LIAO Ning-fang, CUI De-qi, *et al*. Stripe-reduction of the push-broom interferential imaging spectrometer[J]. *Acta Photonica Sinica*, 2011, **40**(4): 587-590.